Research Article

Selective catalytic reduction of nitrogen oxide by ammonia over Cu/SAPO-11: a theoretical study

Beulah Griffe[1,2] · **Joaquín Luis Brito**[1,3] · **Aníbal Sierraalta**[2]

Received: 18 March 2020 / Accepted: 15 June 2020 / Published online: 29 June 2020

Abstract
Quantum chemistry calculations were carried out using the ONIOM2 methodology at two different levels of calculation, B3LYP for the high level and UFF for the low level. These calculations were performed on Cu/SAPO-11, NO–Cu/SAPO-11, NH_3–Cu/SAPO-11 and NO + NH_3–Cu/SAPO-11 to investigate the reaction pathway of the selective catalytic reduction of nitrogen oxides by ammonia in the presence of Cu/SAPO-11. NH_2NO is formed, and then is decomposed into N_2 and H_2O over Cu/SAPO-11 for the catalytic reduction of NO in two steps. The adsorption energy ΔE_{ads} of NO, NH_3 on Cu/SAPO-11 and the change of energy of the reduction reaction are presented. The energy profile of the formation of NH_2NO–Cu/SAPO-H key intermediate is shown. Some relevant charges and bond indexes were calculated. On adsorbing NH_3 or NO on Cu/SAPO-11 there is charge transfer to the aggregates. Vibrational frequencies of adsorbed NH_3, NO and of NH_2NO–Cu/SAPO-11cluster are reported. The importance of adsorbing NH_3 previously to the reduction of NO is emphasized.

Keywords ONIOM · Theoretical calculations · Computational catalysis · Cu-clusters · Cu/SAPO · NH_3-SCR

1 Introduction

Over the last decades, nitrogen oxides (NOx) discharged by motor vehicles and stationary sources are revealed to be dominant air contaminants. The lessening of environmentally dangerous NOx compounds, responsible for the photochemical smog and acid rain, haze and the various options ozone depletion, represents an important task for conservational science and catalysis [1–3]. To control NOx emissions, several technologies have been developed, the selective catalytic reduction of NOx (SCR) with reducing agents (H_2, CO, hydrocarbons and NH_3) to form N_2 and H_2O or CO_2 and H_2O being one of the most encouraging techniques [1–9]. Among the various options, selective catalytic reduction with ammonia (NH_3 – SCR) is the most practical and selective method [1–3, 10, 11].

Applications of copper in catalysis are governed by both the relatively easy reducibility of Cu(II) species, usually the stable precursor ones, and the reversibility among its different oxidation states, principally between Cu(II) and Cu(I). The inorganic matrix employed as support (e.g., alumina, silica, zeolites), also plays an important role [8]. In this regard, the structures of silico-aluminophosphates (SAPO) are attractive materials in catalysis, for being flexible and porous substrates that can accommodate atoms, due to their medium acidic properties and their selectivity. Copper can also form small aggregates and its use as catalyst, supported on different SAPO structures, has been reported [7, 8, 12].

Mathisen et al. [8] described the use of Cu/SAPO-5 and Cu/SAPO-11 catalysts in the selective catalytic reduction (SCR) of NOx by propene. Employing in situ XAS and IR, it was found that in both ion exchanged SAPO-5 and SAPO-11,

✉ Beulah Griffe, beulah.griffe@gmail.com | [1]Laboratorio de Fisicoquímica de Superficies, Centro de Química, IVIC, Apdo. Postal 20632, Caracas 1020-A, Venezuela. [2]Laboratorio de Química-física y Catálisis Computacional, Centro de Química, IVIC, Apdo. Postal 20632, Caracas 1020-A, Venezuela. [3]Universidad Regional Amazónica IKIAM, Tena, Ecuador.

the Cu is present as Cu(II) in a octahedral structure (tetragonally-distorted). A portion of the loaded Cu(II) is reduced thermally in helium, and a further part of Cu(II) is reduced by propene to Cu(I) or to Cu (0) particles. Mathisen and co-workers [8] also outlined that in both catalysts, NOx species oxidize Cu(I) back to Cu(II), however to a fewer extent. They stated that the de-NOx activity of these catalysts is ruled by the high reducibility of Cu(II), the reversibility of the copper valence states and the structural properties of the original material used in the preparation of the catalysts. The authors reported that it is particularly notable that the Cu/SAPO-11 prepared by hydrothermal ion exchange displays a very acute pre-edge signal in XAS analysis that is distinctive of a monomeric linear Cu(I) in a double coordination.

Hoang and coworkers [12] stated that +2 is the original oxidation state of Cu after calcination in air at 400 °C, independently of the type of the support. The Cu^{2+} cations are stabilized in zeolite Y and SAPO-5, while on Al_2O_3 support they are quantitatively reduced by hydrogen to metallic copper. The authors obtained results analogous to Mathisen et al. [8], when comparing the TPR of the samples calcined in air and that of samples treated additionally in argon. In zeolite Y and SAPO-5, the Cu^{2+} cations are stabilized in two distinct forms. The stable Cu^{2+} ions can be reduced in hydrogen to form Cu^{+}, although they are not auto-reduced by pre-treatment in argon at 650 °C. On the other hand, the weakly stabilized Cu^{2+} ions, could be auto-reduced by pre-treatment in argon at 650 °C producing Cu^{+} and become completely reduced in hydrogen to metallic Cu [12].

Xue et al. [7] prepared by ion exchange a series of Cu/SAPO-34 catalyst samples with various Cu contents for selective catalytic reduction of NO by NH_3. The authors concluded that the active sites for the NH_3 SCR reaction, in the temperature range 100–200 °C are specifically the isolated Cu^{2+} sites, in connection with the six-ring window and displaced into the ellipsoidal cavity of SAPO-34 structure.

Li et al. [13] proposed a theoretical study of the NH_3-SCR reaction mechanism over H-form zeolites based on an overall reaction scheme previously suggested by Richter [14] that can be expressed as follows:

$$2NO + O_2 \rightarrow 2NO_2 \quad (1)$$

$$NO + NO_2 \rightarrow N_2O_3 \quad (2)$$

$$N_2O_3 + H_2O \rightarrow 2HNO_2 \quad (3)$$

$$NH_3(ads) + HNO_2 \rightarrow NH_4NO_2(ads) \quad (4)$$

$$NH_4NO_2(ads) \rightarrow NH_2NO(ads) + H_2O \quad (5)$$

$$NH_2NO(ads) \rightarrow N_2 + H_2O \quad (6)$$

The reaction steps (4–6) take place on the Brønsted acid sites of the H-form zeolites [13].

In general, the SCR reaction mechanism of NOx by NH_3 over H-form zeolites consists of the oxidation of NO to NO_2 (or NO_2^-) and the subsequent decomposition of NH_4NO_2 formed by the reaction of adsorbed NH_4^+ and NO_2 (or NO_2^-) [13, 15, 16]. This mechanism also relates to metal exchanged zeolites. Nevertheless, the activation barrier of the decomposition of NH_4NO_2 in the gas phase is about 42.0 kcal/mol [17] being much larger than the apparent activation energy of this SCR reaction measured up to 13–14 kcal/mol [18, 19].

By means of Density Functional Theory calculations, Li et al. [13] found that the selective catalytic reduction of NO involves two sequential steps on H-form zeolites. First, NO is directly oxidized to NO_2 by O_2, followed by the production of N_2O_3 or N_2O_4 by further reaction with NO. Then N_2O_3 and/or N_2O_4 react with NH_3 to form NH_2NO in the gas phase with an activation barrier of 15.6 kcal/mol at 373 °K. NH_2NO decomposes to N_2 and H_2O on the Brønsted acid site by a push–pull hydrogen transfer mechanism. Direct decomposition of NH_2NO in the gas phase goes through a high-energy barrier (more than 32 kcal/mol) [1] by virtue of the trouble of intramolecular hydrogen transfer. Nevertheless, over zeolites, the framework serves as both a hydrogen acceptor and donor, which significantly diminish the energy barrier of the decomposition. Li et al. [13] suggested that NH_2NO is the main intermediary, which comes from the reaction of NH_3 and N_2O_3 (or N_2O_4) rather than the NH_4NO_2. More recently, Mao and co-workers [20] also proposed the NH_2NO species as the intermediate in a DFT study of SCR of NOx by NH_3 over Cu-SAPO-34. Li et al. [21] mentioned a HNNOH species formed from NH_2NO in an experimental and theoretical study of NH_3-SCR on Cu-SAPO-18.

It must be taken into account that different catalytic reactions pathways could occur in the SCR-NH_3 of NO. Either, NH_3 adsorption or NO adsorption could the first step in the reaction mechanism, depending of the metal in the exchanged zeolite catalysts [22]. Further reaction with adsorbed or gas phase reactants would depend on which is the surface species involved in the first step.

We have previously published theoretical studies on small Au-clusters, supported on silico-aluminophospates molecular sieves (SAPO-11) [23]. Similarly, we have reported preliminary theoretical results on Cu/SAPO-11 [24]. In this work we present a theoretical study of Cu/SAPO-11 in the selective catalytic reduction of NO with NH_3 (NO SCR-NH_3). The obtained theoretical results suggest the NH_2NO species as an intermediate on the NH_3-SCR of NO in coincidence with Li et al. [13].

2 Computational details and models

Gaussian-03 program [25] ONIOM2 methodology (our own n-layered integrated molecular orbital and molecular mechanics using the two-layered scheme) was employed to obtain all the geometry optimizations and energy calculations to get the lower energy structures. For the high level (designated by spheres in all Figures), it was utilized the DFT approach, by means of B3LYP functional with the full-electron 3-21G* basis set for H, N and O and LANL2DZ with its pseudo potentials for the rest of the atoms of the SAPO-11 ring, i.e. Si, Al, P, composed by 6 oxo-tetrahedrons and Cu. All reactive and adsorbed molecules were incorporated in the high level. Universal force field approach (UFF) was employed for the low level (represented by sticks in the Figures). H atoms were used as frontier atoms in the ONIOM2 calculations. The silico-aluminophosphates molecular sieves (SAPO) model contains 506 atoms and was already described in preceding works [26–28]. Even though the charge of model of SAPO-11 is neutral, the balance of the valence of SAPO-11 high level (HL) atoms on the model system is negative, to benefit the interaction with Cu [23].

Net charges were determined in accord to the Mülliken approach. The bond indexes (BI) were calculated applying Wiberg BI in the natural atomic orbital basis approximation. Vibrational frequencies of N=O, N–O, NH were also calculated. Frequencies and BI values were calculated using only the high level model. Usually, the quality of the results using ONIOM is analogous to those computed with periodical calculations ([26–28] and references therein) and with the advantageous lower computational cost, as compared with similarly constrained clusters [25]. Furthermore, it has been shown in the literature that the computed adsorption energies with ONIOM method correlate well with experimental results ([28] and references therein). ONIOM calculations reveal the support effect and large distance interactions, which are not considered in the case of the unsupported cluster (the gas phase) [29].

3 Results and discussion

3.1 Cu/SAPO-11 monoatomic model

The optimized most stable structure of Cu/SAPO-11 is shown in Fig. 1. The trends observed in Au/SAPO-11 already reported by Griffe et al. in a previous publication [24] are also reproduced in this work. The Si–O and Al–O bond distances (BD) on the anchoring surface sites are enlarged when passing from SAPO-11 to Cu/SAPO-11. That is, Si–O changes from 1.63 and 1.59, to 1.71 and 1.69 Å and Al-O from 1.75 and 1.67, to 1.79 and 1.79 Å on going from SAPO-11 to Cu/SAPO-11. With respect to the bond angle (BA), there is a contraction; Si-O1-Al is decreased from 142.3° to 133.0° and Si–O33–Al from 157.1° to 137.1° (See Table 1). The rest of properties of the substrate remain almost invariant. Cu interacts with SAPO-11 producing only a localized geometrical rearrangement evidenced by BD and BA changes as has been described previously [24]. The Cu monomeric species displayed in Fig. 1, has

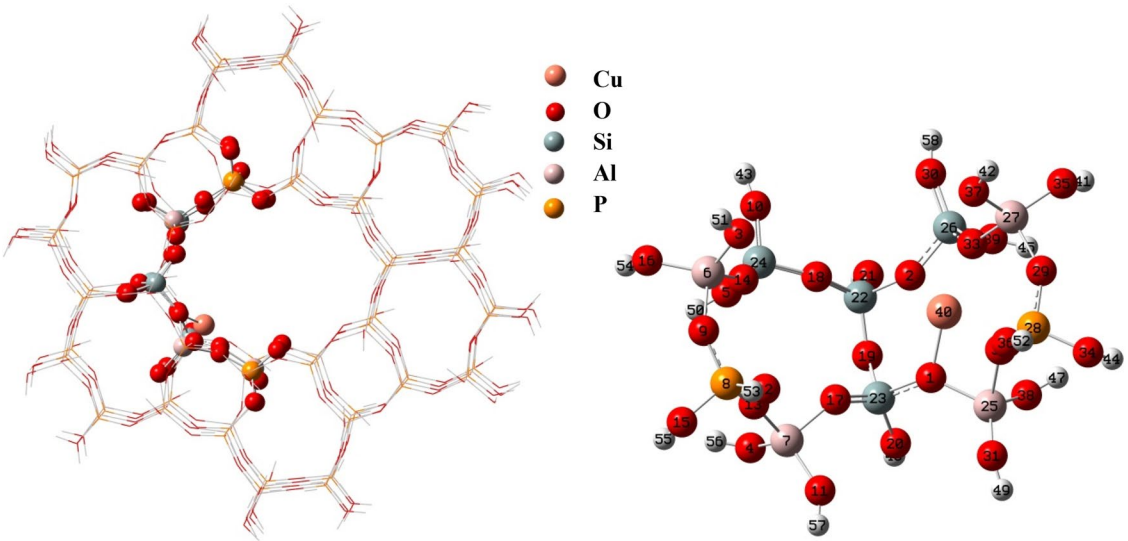

Fig. 1 Left is the optimized lowest energy structure of Cu/SAPO-11 cluster. Right is a detail of the high level atoms

Table 1 Relevant bond distances and angles of SAPO-11, Cu/SAPO-11, NH_3–Cu/SAPO-11, NO–Cu/SAPO-11, and NH_2NO–Cu/SAPO-11-H (See Figs. 1, 2, 3, 4)

Bond/angle	SAPO-11	Cu/SAPO-11	NH_3–Cu/SAPO-11	NO–Cu/SAPO-11	NH_2NO–Cu/SAPO-H
O1–Al25	1.75 Å	1.79 Å	1.81 Å	1.80 Å	1.81 Å
O1–Si23	1.63 Å	1.71 Å	1.70 Å	1.68 Å	1.63 Å
Al25–O1–Si23	142.3°	133.0°	132.7°	132.9°	131.1°
O33–Al27	1.67 Å	1.79 Å	1.78 Å	1.76 Å	1.74 Å
O33–Si26	1.59 Å	1.69 Å	1.68 Å	1.66 Å	1.63 Å
Al27–O33–Si26	157.1°	137.1°	134.2°	138.0°	139.4°
Cu–O1		1.89 Å	1.94 Å	1.98 Å	2.12 Å
Cu–O33		1.98 Å	2.09 Å	2.13 Å	2.33 Å

bond distances of Cu–O1 = 1.89 and Cu–O33 = 1.98 Å respectively.

In Cu/SAPO-11 the net charge of Cu is + 0.88 and the bonding oxygen atoms O1 and O33 of the support are reduced from − 0.9 and − 1.08 in SAPO-11 to − 1.10 in both oxygens in Cu/SAPO-11. Thus, there is charge transference from Cu to the bonding oxygen atoms of the surface. According to BI values in Table 2, the Cu–O1 bond (0.195) is stronger than Cu–O33 bond (0.133).

3.2 Cluster NH_3–Cu/SAPO-11 geometry and adsorption energy

The optimized lowest energy structure resulting from the interaction of NH_3 with Cu/SAPO-11 cluster is shown in Fig. 2.

The NH_3 adsorption presents an energy difference of ΔE_{ads} − 55.11 kcal/mol. The ΔE_{ads} is the energy change, calculated according to the following equation:

$$\text{Cu/SAPO-11} + NH_3 \rightarrow NH_3\text{–Cu/SAPO-11} \quad (7)$$

The NH_3 adsorption energy is defined as:

$$\Delta E_{ads} = E_{NH3\text{–Cu/SAPO-11}} - \left(E_{[Cu/SAPO\text{-}11]} + E_{NH3}\right)$$

where ΔE_{ads} is the NH_3 adsorption energy on Cu/SAPO-11; and $E_{NH3\text{–Cu/SAPO-11}}$, $E_{[Cu/SAPO\text{-}11]}$, and E_{NH3} are the total ONIOM energies of the NH_3–Cu/SAPO-11 and the Cu/SAPO-11 aggregates, and of the free NH_3.

The energy changes ΔE, for all the other equations are calculated in the same way.

The Cu–N BD is 2.0 Å and the N–H BD's are 1.02, 1.04 and 1.02 Å. The interaction of NH_3 with Cu/SAPO-11 has a slight

Table 2 Some relevant calculated properties and net charges of SAPO-11, Cu/SAPO-11, NH_3–Cu/SAPO-11, NO–Cu/SAPO-11 and NH_2NO–Cu/SAPO-11-H aggregates (See Figs. 1, 2, 3, 4)

Charges	SAPO-11	Cu/SAPO-11	NH_3–Cu/SAPO	NO–Cu/SAPO	NH_2NO–Cu/SAPO-H
q_{Cu}		+ 0.88	+ 0.76	+ 0.48	+ 0.41
qb_{O1}	− 0.90	− 1.10	− 1.09	− 1.10	− 1.10
qb_{O33}	− 1.08	− 1.10	− 1.11	− 1.12	− 1.10
q_{N41}			− 0.92 (− 0.82)	+ 0.25 (+ 0.07)	− 0.53 (− 0.51)
$q_{H42, H43}$					+ 0.45, + 0.40 (+0.37, +032)
q_{N45}					+ 0.07 (+ 0.14)
q_{O46}				+ 0.28 (− 0.07)	− 0.24 (− 0.28)
Bond			Bond indexes		
Cu–O1		0.195	0.17	0.11	0.07
Cu–O33		0.133	0.11	0.08	0.04
CuN41(NH_3)			0.27	0.40	0.024
Cu–N45(NO)					0.193
N–O1				0.07	
				2.37	1.622
N–N					1.363

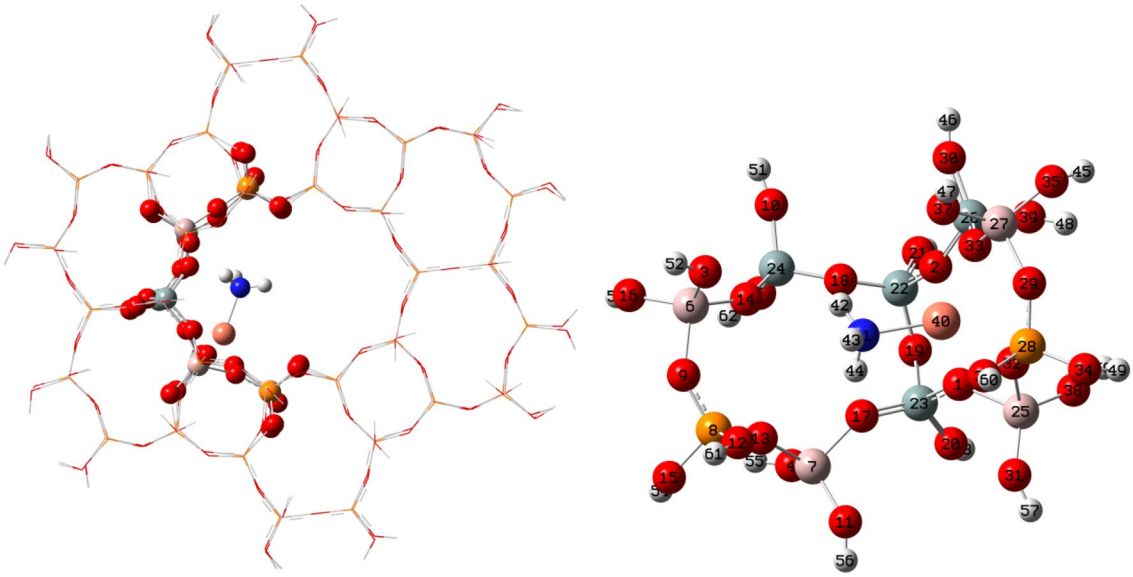

Fig. 2 Left is the optimized minimum energy structure of the interaction of NH_3 with Cu/SAPO-11 cluster. Right is a detail of the high level atoms

influence on the geometrical properties of Cu/SAPO-11 cluster as revealed by Table 1. It is observed that only the Al–O1–Si angle is widened.

Mulliken charges of significant atoms and BI of their bonds were calculated and can be observed in Table 2. The total charge of NH_3 molecule changes from 0.00 in the free species to + 0.39 in the NH_3–Cu/SAPO-11 cluster. Cu atom is reduced from + 0.88 to + 0.76 when passing from Cu/SAPO-11 to NH_3–Cu/SAPO-11, inferring that there is a charge transfer from NH_3 to Cu. Cu–O1 and Cu–O33 BI values diminish to 0.170 au (0.195) and 0.110 au (0.133) due to the interaction Cu–N (0.27 au).

The calculated IR NH_3 absorption frequencies (ν_{NH3}) of the NH_3–Cu/SAPO-11 cluster shows stretching vibration bands of 1296.65; 1673.91; 1736.03; 3086.99; 3467.70; 3997.72; 3999.72; 4001.66 cm^{-1}. The values of the 3086.99–4001.66 range correspond to NH symmetric and anti-symmetric vibrations, 1736 cm^{-1} NH_2 to scissor vibrations and the low vibrational frequencies at 744–370 cm^{-1} range could be due to torsion, rock and waging frequencies [30, 31].

3.3 Cluster NO–Cu/SAPO-11 geometry and adsorption energy

Figure 3 displays the optimized most stable structure resulting from the interaction of NO with Cu/SAPO-11 cluster. The NO is adsorbed on Cu/SAPO-11 with a ΔE = – 57.98 kcal/mol (see Fig. 3) in agreement with Eq. 8.

$$\text{Cu/SAPO-11} + \text{NO} \rightarrow \text{NO–Cu/SAPO-11} \quad (8)$$

Regarding the adsorption energies, ΔE_{NO} is slightly larger than ΔE_{NH3}.

Cu–NO BD is 1.92 Å and the Cu–N–O angle is 136.25°. The interaction of NO with Cu/SAPO-11 produces a decrease in Al–O and Si–O BD and an increase of one of the angles. The adsorption of NO on Cu/SAPO-11 causes a greater effect on some local geometrical properties than that of NH_3 (See Table 1).

Mulliken charges of relevant atoms were calculated (See Table 2). The Cu atom is reduced from + 0.88 in Cu/SAPO-11 to + 0.48 in the NO–Cu/SAPO-11 aggregate after the adsorption of NO molecule, while the free NO molecule charge is oxidized from 0.00 to + 0.53. The O33 is slightly reduced from – 1.10 to – 1.12. Comparing the NH_3 and NO adsorption, the Cu reduction process in NO adsorption is more marked than the NH_3 interaction with Cu. Similarly the oxidation process of NO is more significant than that of the NH_3 in Cu/SAPO-11. BI values presented in Table 2 indicate the Cu–O1 and Cu–O33 weakened bonds (from 0.20 and 0.13 to 0.11 and 0.08 au) due to the enhanced Cu-NO bond (0.40 au). NO BI is 2.37 au as a strong bond and the N has a weak interaction with O1 of the substrate. In conformity to Mulliken charges and BI values, the NO molecule shows a more stable interaction to the surface.

NO–Cu/SAPO-11 is more stable than NH_3–Cu/SAPO-11 (ΔE = – 57.98 kcal/mol vs. – 55.11 kcal/mol). NO–Cu/SAPO 11 hardly reacts with NH_3, although NH_3–Cu/SAPO-11

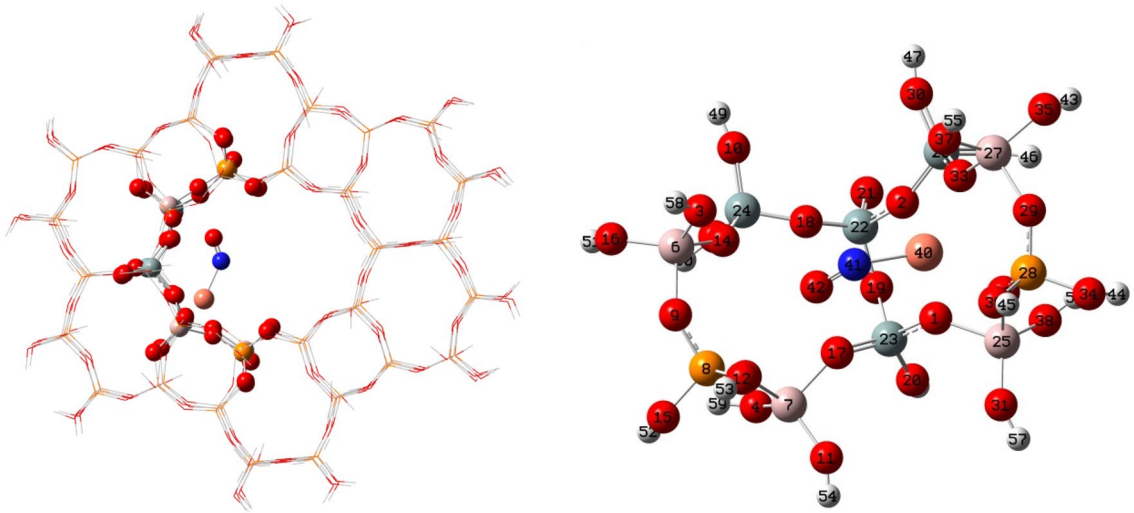

Fig. 3 Left is the optimized most stable structure of the interaction of NO with Cu/SAPO-11 cluster. Right is a detail of the high level atoms

reacts with NO and therefore the reaction of gas-phase NO with NH_3–Cu/SAPO-11 is more suitable and convenient, as it was revealed by our calculations. That is, in our study a pathway comprising as first step the NH_3 adsorption arises since the reaction only occurs when NH_3 is previously adsorbed.

Infrared absorption frequency of NO–Cu/SAPO-11 was calculated and presents a peak at 1915 cm^{-1}. This vibrational frequency agrees with the band experimentally reported at 1904 cm^{-1} assigned to Cu^{+2}–NO species in Cu–ZSM5 and Cu–mordenite catalysts [32, 33]. These studies have suggested that NO coordinates either to Cu(II) or Cu(I) but not to Cu–metal [32, 33].

3.4 The NH_3-SCR of NO in NO + NH_3–Cu/SAPO-11 modeled reaction

In Fig. 4, the optimized lowest energy structure resulting of the selective catalytic reduction of nitrogen monoxide NO with NH_3–Cu/SAPO-11 aggregate is presented. In this figure the Nitrosamide species, NH_2NO, can be noticed. NH_2NO–Cu/SAPO-11-H is attained with a total difference energy of $\Delta E_F = -130.0$ kcal/mol in agreement with Eq. 9.

$$NH_3\text{–Cu/SAPO-11} + NO \rightarrow NH_2NO\text{–Cu/SAPO-11-H} \quad (9)$$

Li et al. [13] and Mao et al. [20] have reported the presence of NH_2NO species. They suggest that the catalytic reduction of NO consists of two consecutive steps on H-form zeolites: First, NO is oxidized to NO_2 by O_2, followed by the formation of N_2O_3 or N_2O_4 which reacts with NH_3 to produce NH_2NO. In our results, the NH_2NO species is obtained directly through the reduction of NO by the NH_3–Cu/SAPO-11 cluster, where one of the H (H44) from NH_3 interacts with the O17 of the substrate (see Fig. 4 right). This fact could suggest that an extraordinary activation of the NH_3 is produced by its interaction with Cu/SAPO-11 substrate, therefore promoting the direct NO reduction.

In NH_2NO–Cu/SAPO- H, i.e., the product of the SCR of NO with NH_3–Cu/SAPO-11 (Table 1), changes upon the reduction reaction occur beyond the atoms/bonds directly linked to Cu, i.e., the O–Si BD's of the substrate are decreased and even the Al27–O33 BD is diminished (see Fig. 4 right).

NH_2NO–Cu/SAPO-11 was calculated after eliminating the H bonded to the O of the substrate of NH_2NO–Cu/SAPO-11-H, that is eliminating H44 (Fig. 4 right) in order to compare with NH_2NO + Cu/SAPO11 adsorption (that is the modeled interaction of free NH_2NO molecule with Cu/SAPO-11) and likewise with the direct decomposition to $N_2 + H_2O$. NH_2NO–Cu/SAPO-11 assembly is very similar to the most stable structure resulting from Cu/SAPO-11 + NH_2NO interaction displayed in Fig. 5, not only by comparing the geometrical properties but also from the point of view of the calculated properties, as it is presented in Table 3. The charges and bond indexes of some selected bonds of NH_2NO–Cu/SAPO-11 and NH_2NO + Cu/SAPO species are quite similar. This feature validates the presence of the NH_2NO species in our calculation and its direct attainment through the reduction of NO by the NH_3–Cu/SAPO-11 cluster, since when the remaining H is eliminated the two clusters are comparable. The difference of Cu charge in NH_2NO–Cu/SAPO-11-H (+ 0.41) with respect to NH_2NO–Cu/SAPO-11 and NH_2NO + Cu/

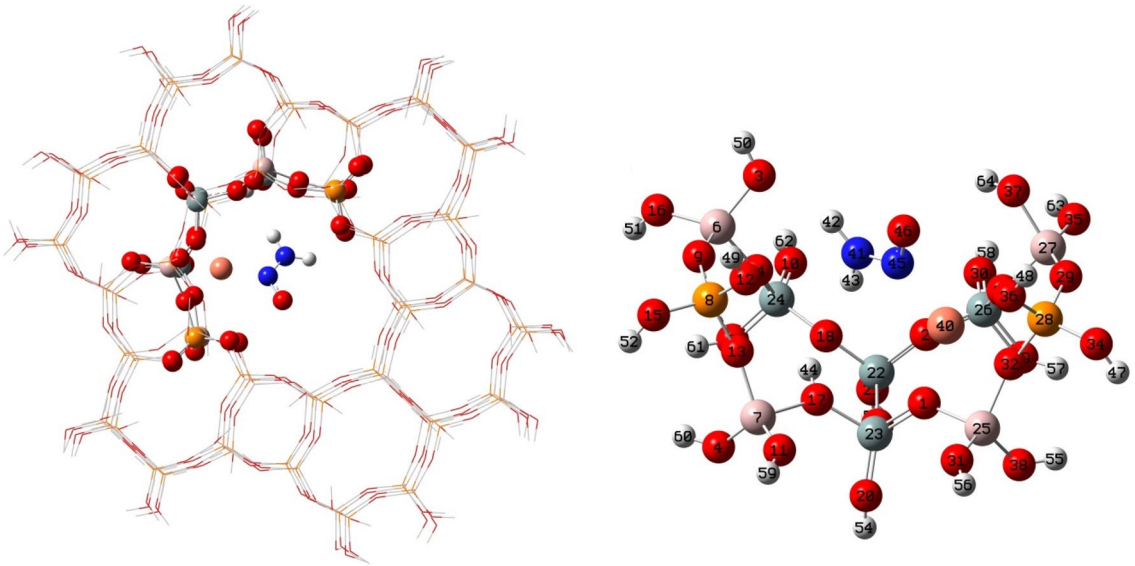

Fig. 4 Left is the lowest energy structure of the reaction of NH_3–Cu/SAPO-11 cluster with NO. Right is a detail of the high level atoms

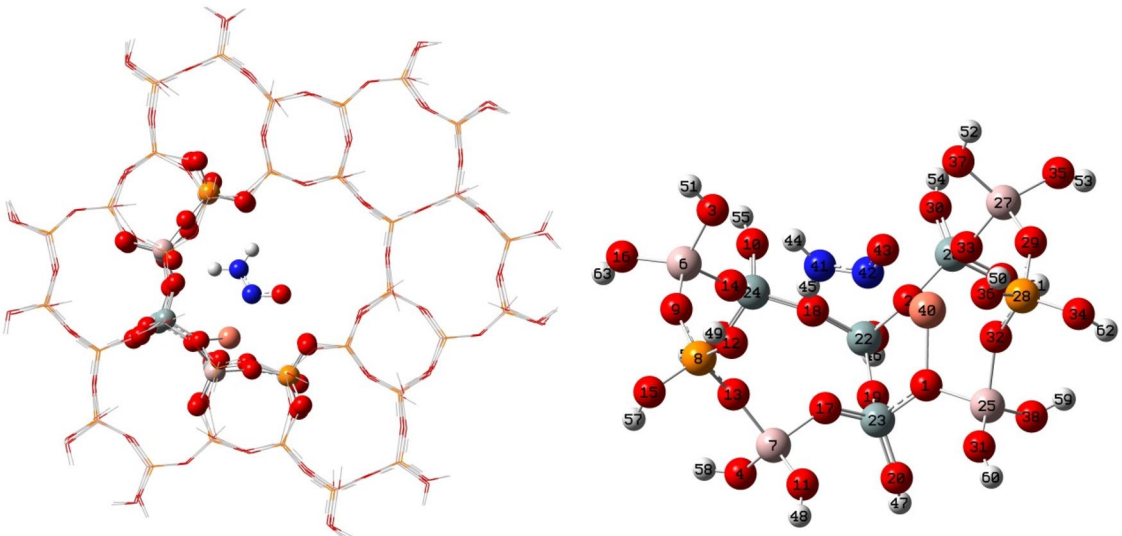

Fig. 5 Left is the optimized lowest energy structure of NH_2NO + Cu/SAPO-11cluster obtained by reaction of Cu/SAPO-11 + NH_2NO. Right is a detail of the high level atoms

SAPO (+ 0.82) is due to the presence of the H atom from de NH_3 in the first aggregate.

The decomposition process of the NH_2NO–Cu/SAPO-11 to form N_2 and H_2O was calculated and shows an energy change of $\Delta E = -33.7$ kcal/mol. The products of the decomposition reaction are more stable than the intermediate species (See Fig. 6) according to Eq. 10:

$$NH_2NO\text{–Cu/SAPO-11} \rightarrow N_2 + H_2O + \text{Cu/SAPO-11} \quad (10)$$

Thus, the NH_2NO decomposition to $N_2 + H_2O$ is favored by the Cu/SAPO-11 structure.

Li [13] proposed that the SCR reaction of NOx consists of two successive stages. The first leads to formation of

Table 3 Some relevant calculated properties and net charges of NH_2NO, NH_2NO–Cu/SAPO-H, NH_2NO + Cu/SAPO and NH_2NO–Cu/SAPO-11

Charges	NH_2NO	NH_2NO–Cu/SAPO-11-H	NH_2NO + Cu/SAPO	NH_2NO–Cu/SAPO
qCu		+0.41	+0.82	+0.81
qbO1		−1.10	−1.09	−1.09
qbO33		−1.10	−1.10	−1.10
qN41	−0.51	−0.53	−0.49	−0.48
qH42	+0.32	+0.45	+0.44	+0.44
qH43	+ 0.34	+ 0.40	+0.48	+0.48
qN45	+0.14	+0.07	+0.12	+0.11
qO46	−0.28	−0.24	−0.22	−0.23
Bond		Indexes		
Cu–O1		0.07	0.16	0.16
Cu–O33		0.04	0.10	0.10
Cu–N41		0.02	0.02	0.014
N41–H42	0.80	0.74	0.73	0.73
N41–H43	0.81	0.78	0.73	0.73
Cu–N45(NO)		0.19	0.18	0.18
N45–O1		0.01	0.01	0.01
N45–O46	1.71	1.62	1.57	1.57
N–N	1.34	1.36	1.45	1.45

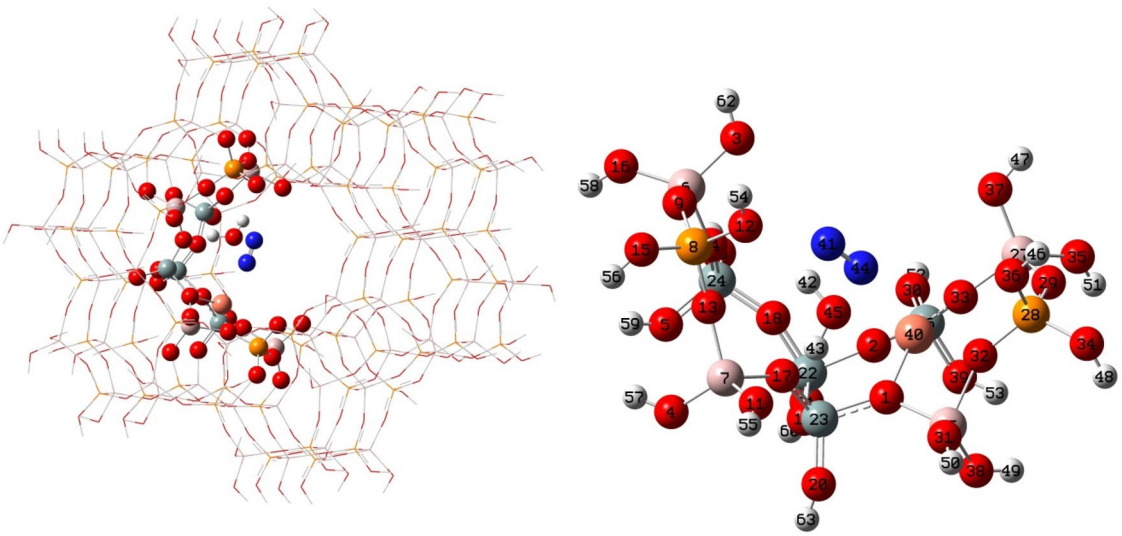

Fig. 6 Left is the ground state optimal geometry of **(**$N_2 + H_2O$) + Cu/SAPO-11 obtained by reduction of the obtained specie NH_2NO-Cu/SAPO-11. Right is a detail of the high level atoms

NH_2NO in the gas phase. The second stage is the catalytic decomposition of NH_2NO to produce $N_2 + H_2O$. This proposed mechanism comprises 4 steps. Richter et al. [14] suggested an overall reaction pathway of 6 steps. Our model includes only two overall steps, since NO is directly reduced to $NH_2NO + H$, bypassing the oxidation of NO to NO_2 by O_2, and the formation of N_2O_3 or N_2O_4 which would react with NH_3 to produce NH_2NO.

Li [13] reported that the presence of sufficient Brönsted acid sites on the exchanged H-form zeolites ensures the push–pull hydrogen transfer mechanism. A new route for formation of NH_2NO with low activation energy might enhance the SCR activity of zeolite based catalysts [13].

In the present study the Cu/SAPO-11 is shown to serve as both, a hydrogen acceptor and donor, which significantly promotes the formation of the NH_2NO–Cu/SAPO-11-H

(Fig. 4) and posterior decomposition to N_2 and H_2O (Fig. 6). In NH_2NO–Cu/SAPO-11-H, an H from the NH_3 is bonded to an O of the substrate (H44–O17 in Fig. 4 right) confirming the H acceptor behavior of Cu/SAPO-11. In the same way this substrate could enhance a low activation energy decomposition of NH_2NO to $N_2 + H_2O$ for the motives presented above. Particularly the NH_3–Cu/SAPO-11 aggregate activation is fundamental to the first stage, by achieving the NH_2NO species.

Table 4 displays the calculated vibrational frequencies in cm^{-1} for NH_2NO–Cu/SAPO-11, NH_2NO + Cu/SAPO (see Fig. 5) and NH_2NO. The assignments presented in Table 4 are based on those reported by Harrison [31]. The most important calculated frequencies of NH_2NO–Cu/SAPO-11 and NH_2NO + Cu/SAPO are coincident with those reported by Harrison at 3520, 3357, 1675, 1585, 1239, 1113, 662, 614 and 329 cm^{-1} [31]. The frequencies disclosed on Table 4 also confirm the presence of NH_2NO species in the NH_2NO–Cu/SAPO-11 and NH_2NO–Cu/SAPO-11-H aggregates.

3.5 Formation mechanism of NH_2NO–Cu/SAPO-H

The transition state of the formation of NH_2NO–Cu/SAPO-H was calculated using the synchronous transit-guided quasi-Newton QST2 method included in the Gaussian package [25]. The reaction path that connects the transition state with the respective product and reactants were achieved using the intrinsic reaction coordinates (IRC) calculations (see Fig. 7a).

We have the following reactions in agreement with our calculations:

$$NH_3\text{–Cu/SAPO} + NO \rightarrow NH_2\text{–NO–Cu/SAPO-H(TS)} \quad (11)$$

$$NH_2\text{–NO–Cu/SAPO–H(TS)} \rightarrow NH_2NO\text{–Cu/SAPO-H} \quad (12)$$

The activation energy for Reaction 11 is $\Delta E^{\pm} = +61.34$ kcal/mol, then the transition state NH_2–NO–Cu/SAPO-H(TS) relax to the product (Reaction 12) with an energy change $\Delta E = -191.34$ kcal/mol. The optimized structures of the minima and the transition state are shown in Fig. 7a and the energy profile for the formation of NH_2NO–Cu/SAPO-H is displayed in Fig. 7b.

The large energy change ΔE of the transition state relaxation to the product, confirms the significant role of the substrate that serves as a hydrogen acceptor, promoting the formation of the NH_2NO-Cu/SAPO-11-H (Figs. 4, 7a, b) and posterior decomposition to N_2 and H_2O (Fig. 6) as stated in Sect. 3.4. In NH_2NO–Cu/SAPO-11-H, an H atom from the NH_3 is bonded to an O atom of the substrate (H44–O17 in Fig. 4 right) corroborating the H acceptor behavior of Cu/SAPO-11. We suggest that the NH_2NO–Cu/SAPO-H is the key intermediate in the formation of NH_2NO in our calculated model.

Table 4 Calculated vibrational frequencies in cm^{-1} of NH_2NO–Cu/SAPO, NH_2NO + Cu/SAPO and NH_2NO

Assignment	NH_2NO–Cu/SAPO	NH_2NO + Cu/SAPO	NH_2NO
NHa-str	3505	3519	3644
NHs-str	3316	3290	3417
NOstr/NNH_2bend	1659	1659	1606
NH_2sci	1444	1478	1378
NH_2bend/NNH-$_2$bend	1262	1283	1136
NNH_2bend/NNstr	1225, 1152	1227, 1162	
NH_2 torsion	566	553	551
NH_2 rock	488	498	
NH_2 wag	476	471	434

3.6 The modeled N_2O_3–Cu/SAPO-11

The first two steps of the overall reaction pathway proposed by Richter [14] and commented by Li [13] have been modeled on Cu/SAPO-11:

$$NO\text{–Cu/SAPO-11} + O \rightarrow NO_2\text{–CuSAPO-11} \quad (13)$$

$$NO_2\text{–CuSAPO-11} + NO \rightarrow N_2O_3\text{–CuSAPO-11} \quad (14)$$

with the purpose of reproducing part of the mechanism described by Li [13] and mentioned above, consisting of two consecutive steps. The first step involves the direct oxidation of NO to NO_2 and the subsequent combination of NO_2–CuSAPO-11 with another NO molecule to give N_2O_3–CuSAPO-11.

The N_2O_3–CuSAPO-11 model coming from the two steps proposed by Richter is attained [14], however, the second reaction does not proceed straightforward. The N–N BD in N_2O_3–CuSAPO-11 is larger than reported for pure N_2O_3 (1.95 Å vs. 1.85–1.89 Å) [34–36]. This aggregate was calculated and the difference energy of ΔE is large, given that, the first step NO–Cu/SAPO + O presents a great energy difference (see Fig. 8). In the second step, the NO_2–CuSAPO-11 cluster is stable and therefore the reaction with the NO molecule is achieved but not straightaway.

The reaction:

$$N_2O_3 + \text{Cu/SAPO-11} \rightarrow N_2O_3 + \text{Cu-SAPO-11} \quad (15)$$

was also calculated and modeled. The optimized lowest energy structure of N_2O_3 + Cu/SAPO-11 cluster is shown in Fig. 9. The difference energy ΔE of this reaction is −65.95 kcal/mol.

In Table 5 it is indicated a comparative Cu–O and other relevant interactions, charges of N_2O_3, N_2O_3–Cu/SAPO and

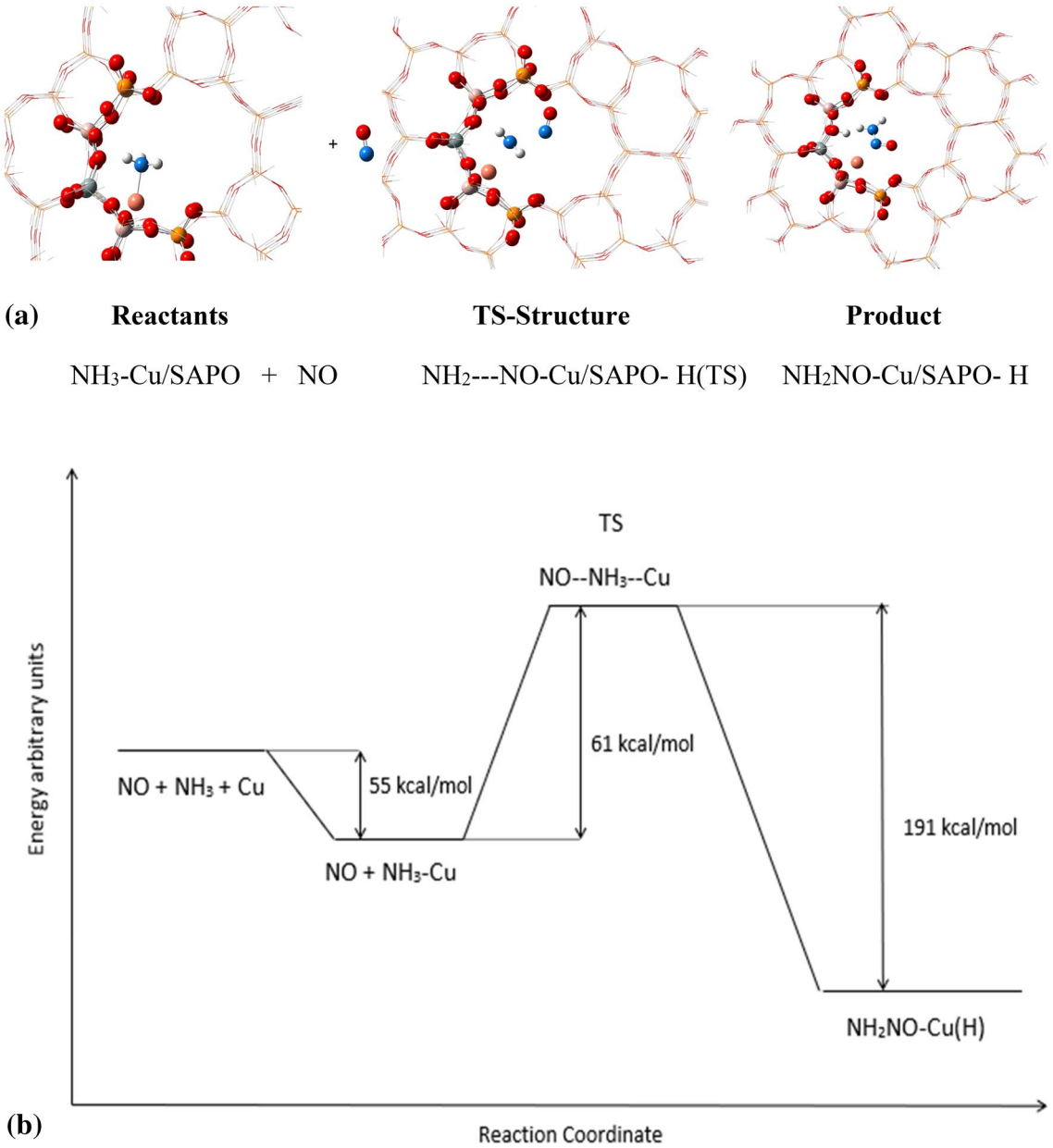

Fig. 7 **a** Geometries of minima and transition state involved in the formation of NH_2NO-Cu/SAPO-11. **b** Energy profile of the NO + NH_3 + Cu/SAPO-11 modeled reaction

N_2O_3 + Cu/SAPO. Although the geometries of these aggregates are not identical, as shown in Figs. 8 and 9, there are similarities in common bonds, suggesting that the N_2O_3 species could also be obtained on Cu/SAPO, although not by a direct reaction.

4 Conclusions

DFT calculations have been performed to investigate the possible mechanism of the SCR of NO by NH_3 over Cu/

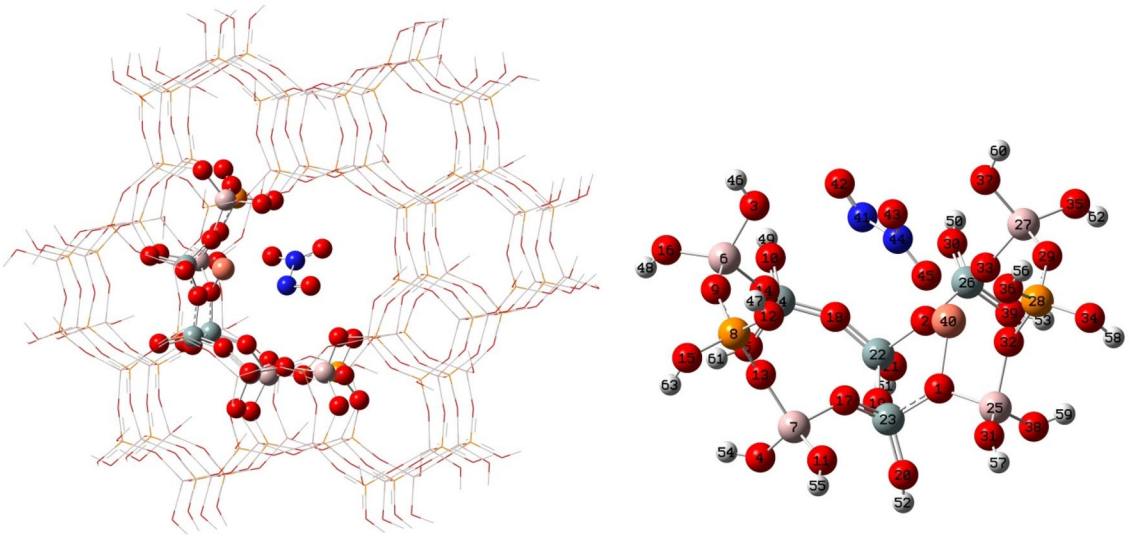

Fig. 8 Left is the optimized lowest energy structure of N_2O_3–Cu/SAPO-11 cluster obtained by reaction of NO_2–Cu/SAPO-11 + NO. Right is a detail of the high level atoms

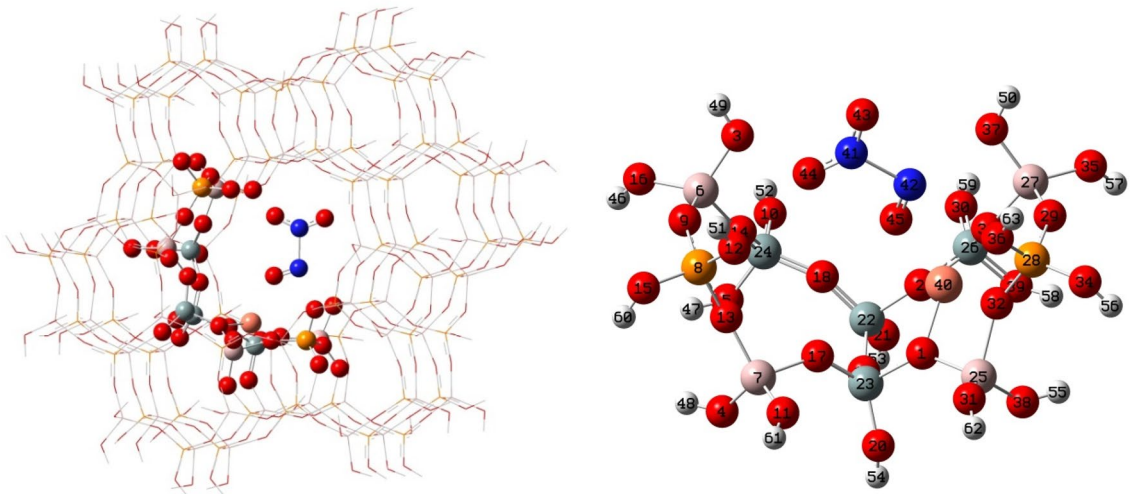

Fig. 9 Left is the ground state optimal geometry of N_2O_3 + Cu/SAPO-11 cluster obtained by reaction of Cu/SAPO-11 + N_2O_3. Right is a detail of the high level atoms

SAPO-11. The geometry optimizations and energy calculations were done using Gaussian-03 program ONIOM2 methodology by means of the two-layer model. It was shown that Cu interacts with SAPO-11 producing a localized geometrical rearrangement evidenced by BD and BA changes and charge transfer from Cu to the bonding oxygen atoms on the surface. The interaction of NH_3 with Cu/SAPO-11 (NH_3–Cu/SAPO) has a minor influence on the geometrical properties of Cu/SAPO-11 cluster. NH_3 gas does not react with NO in NO–Cu/SAPO-11, whereas NO gas is reduced by NH_3-Cu/SAPO-11. Therefore, the reaction of NO with NH_3–Cu/SAPO-11 is more probable, suggesting that NH_3 should be previously adsorbed on Cu/SAPO. The Cu/SAPO-11 cluster could function by a push–pull hydrogen transfer mechanism that serves as both, a hydrogen acceptor and donor, which significantly favors the formation of the NH_2NO–Cu/SAPO-11-H and its posterior catalytic decomposition to N_2 and H_2O. This fact is corroborated by the calculation of NH_2… NO–Cu/SAPO-H(TS) with a large energy change ΔE of the transition state relaxation to the product, verifying the significant role of the substrate. The reaction pathway of

Table 5 Some relevant calculated properties and net charges of N_2O_3, N_2O_3–Cu/SAPO and N_2O_3 + Cu/SAPO

Charges	N_2O_3	N_2O_3–Cu/SAPO	N_2O_3 + Cu/SAPO
qCu		+0.80	+0.81
qbO1		−1.10	−1.10
qbO33		−1.11	−1.10
qN41	+0.14	+0.29	+0.17
O42	−0.16	+0.08	+0.05
qO43	−0.17	−0.13	−0.18
qN44	+0.19	+0.19	+0.23
qO45	−0.01	−0.29	−0.08
Bond	Bond indexes		
Cu–O1		0.18	0.18
Cu–O33		0.11	0.12
Cu–N41		< 0.01	< 0.01
Cu–N44		0.01	0.01
N41–N44	0.50	0.42	0.55
N41–O42	1.59	2.25	1.55
N44–O43	1.57	1.68	1.62
N44–O45	2.16	1.39	2.04
N–N			

In the case of N_2O_3 and N_2O_3 + Cu/SAPO N44–O45 corresponds to N=O while in the case of –N_2O_3–Cu/SAPO N41–O42 is the N=O

SCR-NH_3 of NO proposed in this study via NH_2NO species consists of two steps, vis-à-vis previous mechanisms of four and six steps in SCR of NOx on H-zeolites. In the first step NH_2NO composite is obtained straightforward by the reduction of NO by the NH_3–Cu/SAPO-11 cluster. In the second step the decomposition of NH_2NO to N_2 and H_2O is achieved. Vibrational frequencies of the most significant species are calculated and serve to identify the intermediate compounds and to endorse the presence of NH_2NO species.

Compliance with ethical standards

Conflict of interest The authors declare that they have no conflict of interest.

References

1. Mao Y, Wang HF, Hu P (2015) Theoretical investigation of NH_3-SCF over zeolites: a review. Int J Quantum Chem 115:618–630. https://doi.org/10.1002/qua.24844
2. Can F, Courtois Z, Royer S, Blanchard G, Rousseau S, Duprez D (2012) An overview of the production and use of ammonia in NSR + SCR coupled system for NO_x reduction from lean exhaust gas. Catal Today 197:144–154. https://doi.org/10.1016/j.cattod.2012.07.032
3. Fu M, Li C, Lu P, Qu L, Zhang M, Zhou Y, Yu M, Fang Y (2014) A review on selective catalytic reduction of NO_x by supported catalysts at 100–300 °C—catalysts, mechanism kinetics. Catal Sci Technol 4:14–25. https://doi.org/10.1039/c3cy00414g
4. Forzatti P (2001) Present status and perspectives in de-NO_x SCR catalysis. Appl Catal A Gen 222:221–236. https://doi.org/10.1016/S0926-860X(01)00832-8
5. Liu J, Li X, Zhao Q, Hao C, Zhang D (2013) Insight into the mechanism of selective catalytic reduction of NO_x by propene over the $Cu/Ti_{0.7}Zr_{0.3}O_2$ catalyst by Fourier transform Infrared spectroscopy and density functional theory calculations. Environ Sci Technol 47:4528–4535. https://doi.org/10.1021/es3049898
6. Hamada H, Haneda M (2012) A review of selective catalytic reduction of nitrogen oxides with hydrogen and carbon monoxide. Appl Catal A Gen 421–422:1–13. https://doi.org/10.1016/j.apcata.2012.02.005
7. Xue J, Wang X, Qi G, Wang J, Shen M, Li W (2013) Characterization of copper species over Cu/SAPO-34 in selective catalytic reduction of NO_x with ammonia: relationships between active Cu sites and de-NO_x performance at low temperature. J Catal 297:56–64. https://doi.org/10.1016/j.jcat.2012.09.020
8. Mathisien K, Stockenhuber M, Nicholson DG (2009) In situ XAS and IR studies on Cu:SAPO-5 and Cu:SAPO-11: the contributory role of monomeric linear copper(I) species in the selective catalytic reduction of NO_x by propene. Phys Chem Chem Phys 11:5476. https://doi.org/10.1039/b902491c
9. Shi N, Tu B, Sun W, Liu J, Cao L, Gong X, Yang J (2016) Room temperature efficient reduction of NO_x by H_2 in a permeable compounded membrane –Catalytic reactor. Chem Eng J 283:929–935. https://doi.org/10.1016/j.cej.2015.08.062
10. Liu F, Yu Y, He H (2014) Environmentally-benign catalysts for the selective catalytic reduction of NO_x from diesel engines: structure–activity relationship and reaction mechanism aspects. Chem Commun 50:8445–8463. https://doi.org/10.1039/c4cc01098a

11. Li J, Chang H, Ma L, Hao J, Yang R (2011) Low-temperature selective catalytic reduction of NOx with NH_3 over metal oxide and zeolite catalysts—a review. Catal Today 175:147–156. https://doi.org/10.1016/j.cattod.2011.03.034
12. Hoang DL, Dang T, Engeldinger J, Schneider M, Radnik J, Richter M, Martin A (2011) TPR investigations on the reducibility of Cu supported on Al_2O_3, zeolite Y and SAPO-5. J Solid State Chem 184:1915–1923. https://doi.org/10.1016/j.jssc.2011.05.042
13. Li J, Li S (2007) New insight into selective catalytic reduction of nitrogen oxides by ammonia over H-form zeolites: a theoretical study. Phys Chem Chem Phys 9:3304–3311. https://doi.org/10.1039/b700161d
14. Richter M, Eckelt R, Parlitz B, Fricke R (1998) Low-temperature conversion of NO, to N_2 by zeolite-fixed ammonium ions. Appl Catal B Environ 15:129–146. https://doi.org/10.1016/S0926-3373(97)00042-8
15. Sun Q, Gao ZX, Chen HY, Sachtler WMH (2001) Reduction of NO_x with ammonia over Fe/MFI: reaction mechanism based on isotopic labeling. J Catal 201:89–99. https://doi.org/10.1006/jcat.2001.3228
16. Sun Q, Gao ZX, Wen B, Sachtler WMH (2002) Spectroscopic evidence for a nitrite intermediate in the catalytic reduction of NO_x with ammonia. Catal Lett 78:1–5. https://doi.org/10.1023/A:1014981206924
17. Delahay G, Villagomez E, Ducere J, Berthomieu D, Goursot A, Coq B (2002) Selective catalytic reduction of NO by NH_3 on Cu-Faujasite catalysts: an experimental and quantum chemical approach. Chem Phys Chem 3:686–692. https://doi.org/10.1002/1439-7641
18. Andersson L, Brandin J, Odenbrand C (1989) Selective catalytic reduction of NO over acid-leached mordenite catalysts. Catal Today 4:173–185. https://doi.org/10.1016/0920-5861(89)85049-7
19. Brandin J, Andersson L, Odenbrand C (1989) Catalytic reduction of nitrogen oxides on modernite some aspect on the mechanism. Catal Today 4:187–203. https://doi.org/10.1016/0920-5861(89)85050-3
20. Mao Y, Wang Z, Wang WF, Hu P (2016) Understanding catalytic reactions over zeolites: a density functional theory study of selective catalytic reduction of NO_x by NH_3 over Cu-SAPO-34. ACS Catal 6:7882–7891. https://doi.org/10.1021/acscatal.6b01449
21. Li Y, Deng J, Song W, Liu J, Zhao Z, Gao M, Wei Y, Zhao L (2016) Nature of Cu species in Cu – SAPO-18 catalyst for NH_3–SCR: combination of experiments and DFT calculations. J Phys Chem C 120:14669–14680. https://doi.org/10.1021/acs.jpcc.6b03464
22. Rudolph J, Jacob CR (2019) Computational insights into the mechanism of the selective catalytic reduction of NO_x: Fe- versus Cu-exchanged zeolite catalysts. ACS Omega 4:7987–7993. https://doi.org/10.1021/acsomega.9b00600
23. Griffe B, Brito JL, Sierraalta A (2014) Theoretical study of CO adsorption and oxidation on Au_{3-5} clusters supported on silica-aluminophospates. Comput Theor Chem 1042:69–83. https://doi.org/10.1016/j.comptc.2014.05.003
24. Griffe B, Brito JL, Sierraalta A (2017) Comparative theoretical study of Au_{1-3} and Cu_{1-3} clusters supported on SAPO-11 and their interactions with CO. J Comput Methods Sci Eng 17:89–96. https://doi.org/10.3233/JCM-160664
25. Frisch MJ, Trucks GW, Schlegel HB, Scuseria GE, Robb MA, Cheeseman JR, Montgomery JA Jr, Vreven T, Kudin KN, Burant JC, Millam JM, Iyengar SS, Tomasi J, Barone V, Mennucci B, Cossi M, Scalmani G, Rega N, Petersson GA, Nakatsuji H, Hada M, Ehara M, Toyota K, Fukuda R, Hasegawa J, Ishida M, Nakajima T, Honda Y, Kitao O, Nakai H, Klene M, Li X, Knox JE, Hratchian HP, Cross JB, Bakken V, Adamo C, Jaramillo J, Gomperts R, Stratmann RE, Yazyev O, Austin AJ, Cammi R, Pomelli C, Ochterski JW, Ayala PY, Morokuma K, Voth GA, Salvador P, Dannenberg JJ, Zakrzewski VG, Dapprich S, Daniels AD, Strain MC, Farkas O, Malick DK, Rabuck AD, Raghavachari K, Foresman JB, Ortiz JV, Cui Q, Baboul AG, Clifford S, Cioslowski J, Stefanov BB, Liu G, Liashenko A, Piskorz P, Komaromi I, Martin RL, Fox DJ, Keith T, Al-Laham MA, Peng CY, Nanayakkara A, Challacombe M, Gill PMW, Johnson B, Chen W, Wong MW, Gonzalez C, Pople JA (2004) Gaussian 03, Revision D. 02. Gaussian Inc., Wallingford
26. Sierraalta A, Añez R, Ehrmann E (2007) ONIOM study of Ga/SAPO-11 catalyst: species formation and reactivity. J Mol Catal A: Chem 271:185–191. https://doi.org/10.1016/j.molcata.2007.03.002
27. Griffe B, Sierraalta A, Brito JL (2009) Theoretical study of the water effect on CO adsorbed over Au/SAPO-11 catalysts. J Comput Methods Sci Eng 9:281–287. https://doi.org/10.3233/JCM-2009-0303
28. Griffe B, Brito JL, Sierraalta A (2010) Theoretical study of Au/SAPO-11 catalyst and its potential use in thiophene HDS. J Mol Catal A: Chem 315:28–34. https://doi.org/10.1016/j.molcata.2009.08.010
29. Joshi AM, Delgass NW, Thomson KT (2007) Interaction of carbon monoxide with small gold clusters inside TS-1 pores. J Phys Chem C 111:11424–11436. https://doi.org/10.1021/jp072833i
30. Stevens RM (1971) Accurate SCF Calculation for ammonia and its inversion motion. J Chem Phys 55:1725–1729. https://doi.org/10.1063/1.1676303
31. Harrinson JA, Maclagan RG, White AR (1986) The structure and vibrational frequencies of NH_2NO. Chem Phys Lett 130:98–102. https://doi.org/10.1016/0009-2614(86)80433-X
32. Cheung T, Bhargava SK, Hobday M, Foger K (1996) Adsorption of NO on Cu exchanged zeolites, an FTIR study: effects of Cu levels, NO pressure, and catalyst pretreatment. J Catal 158:301–310. https://doi.org/10.1006/jcat.1996.0029
33. Hoost TE, Laframboise KA, Otto K (1995) NO adsorption on Cu-ZSM-5: assignment of IR band at 2133. Catal Lett 33:105–116. https://doi.org/10.1007/BF00817050
34. Simon A, Horakh J, Obermeyer A, Borrmann H (1992) Crystalline nitrogen oxides-crystal structure of N_2O_3 and a remark concerning the crystal structure of N_2O_5. Angew Chem Int Ed Engl 31:301–303. https://doi.org/10.1002/anie.199203011
35. Horakh J, Borrmann H, Simon A (1995) Phase relationships in the N_2O_3/N_2O_4 system and crystal structures of N_2O_3. Chem Eur J 1:389–393. https://doi.org/10.1002/chem.19950010610
36. Solans-Monfort X, Branchadell V, Sodupe M (2000) Theoretical study of the structure of $ZCu(NO_2)(NO)$. A proposed intermediate in the NO*x* decomposition by Cu-ZSM-5. J Phys Chem A 104:3225–3230. https://doi.org/10.1021/jp993798l